SUBMILLIMETER GALAXIES AS PROGENITORS OF COMPACT QUIESCENT GALAXIES

S. TOFT[1], V. SMOLČIĆ[2], B. MAGNELLI[3], A. KARIM[3,4], A. ZIRM[1], M. MICHALOWSKI[5,6,18], P. CAPAK[7,8], K. SHETH[9],
K. SCHAWINSKI[10], J.-K. KROGAGER[1,11], S. WUYTS[12], D. SANDERS[13], A. W. S. MAN[1], D. LUTZ[12], J. STAGUHN[12,14], S. BERTA[12],
H. MCCRACKEN[15], J. KRPAN[2], AND D. RIECHERS[16,17]

[1] Dark Cosmology Centre, Niels Bohr Institute, University of Copenhagen, Juliane Mariesvej 30, DK-2100 Copenhagen, Denmark; sune@dark-cosmology.dk
[2] Physics Department, University of Zagreb, Bijenička cesta 32, 10002 Zagreb, Croatia
[3] Argelander Institute for Astronomy, Auf dem Hügel 71, Bonn, D-53121, Germany
[4] Institute for Computational Cosmology, Durham University, South Road, Durham, DH1 3LE, UK
[5] Scottish Universities Physics Alliance, Institute for Astronomy, University of Edinburgh, Royal Observatory, Edinburgh, EH9 3HJ, UK
[6] Sterrenkundig Observatorium, Universiteit Gent, Krijgslaan 281 S9, B-9000 Gent, Belgium
[7] Spitzer Science Center, 314-6 Caltech, 1201 East California Boulevard, Pasadena, CA 91125, USA
[8] Department of Astronomy, 249-17 Caltech, 1201 East California Boulevard, Pasadena, CA 91125, USA
[9] National Radio Astronomy Observatory, 520 Edgemont Road, Charlottesville, VA 22903, USA
[10] ETH Zurich, Institute for Astronomy, Department of Physics, Wolfgang-Pauli-Strasse 27, CH-8093 Zurich, Switzerland
[11] European Southern Observatory, Alonso de Cordova 3107, Vitacura, Casilla 19001, Santiago 19, Chile
[12] MPE, Postfach 1312, D-85741 Garching, Germany
[13] Institute for Astronomy, 2680 Woodlawn Drive, University of Hawaii, Honolulu, HI 96822, USA
[14] The Henry A. Rowland Department of Physics and Astronomy, Johns Hopkins University, 3400 N. Charles Street, Baltimore, MD 21218, USA
[15] Institut dAstrophysique de Paris, UMR7095 CNRS, Universite Pierre et Marie Curie, 98 bis Boulevard Arago, F-75014 Paris, France
[16] Department of Astronomy, Cornell University, 220 Space Sciences Building, Ithaca, NY 14853, USA
[17] Astronomy Department, California Institute of Technology, MC 249-17, 1200 East California Boulevard, Pasadena, CA 91125, USA

ABSTRACT

Three billion years after the big bang (at redshift $z = 2$), half of the most massive galaxies were already old, quiescent systems with little to no residual star formation and extremely compact with stellar mass densities at least an order of magnitude larger than in low-redshift ellipticals, their descendants. Little is known about how they formed, but their evolved, dense stellar populations suggest formation within intense, compact starbursts 1–2 Gyr earlier (at $3 < z < 6$). Simulations show that gas-rich major mergers can give rise to such starbursts, which produce dense remnants. Submillimeter-selected galaxies (SMGs) are prime examples of intense, gas-rich starbursts. With a new, representative spectroscopic sample of compact, quiescent galaxies at $z = 2$ and a statistically well-understood sample of SMGs, we show that $z = 3$–6 SMGs are consistent with being the progenitors of $z = 2$ quiescent galaxies, matching their formation redshifts and their distributions of sizes, stellar masses, and internal velocities. Assuming an evolutionary connection, their space densities also match if the mean duty cycle of SMG starbursts is 42^{+40}_{-29} Myr (consistent with independent estimates), which indicates that the bulk of stars in these massive galaxies were formed in a major, early surge of star formation. These results suggest a coherent picture of the formation history of the most massive galaxies in the universe, from their initial burst of violent star formation through their appearance as high stellar-density galaxy cores and to their ultimate fate as giant ellipticals.

Key words: cosmology: observations – galaxies: evolution – galaxies: high-redshift – galaxies: starburst – Galaxy: formation – submillimeter: galaxies

Online-only material: color figures

1. INTRODUCTION

One of the most remarkable discoveries in galaxy evolution studies in the past years is that up to half of the most massive galaxies ($\log(M_*/M_\odot) > 11$) at $z \approx 2$ are old, quiescent systems with extremely compact structures, characteristics that correspond to stellar densities that are orders of magnitude higher than what is seen in local elliptical galaxies (e.g., Toft et al. 2007; van Dokkum et al. 2008; Szomoru et al. 2012). Much effort has gone into confirming their extreme properties and investigating their evolutionary path to the local universe. Virial arguments and simulations indicate that the most important process is likely to be minor dry merging (e.g., Bezanson et al. 2009; Oser et al. 2012; Cimatti et al. 2012; Toft et al. 2012), but observations suggest that other processes are likely also important, e.g., the continuous addition of increasingly larger, newly quenched galaxies to the quenched population with decreasing redshift (e.g., Newman et al. 2012; Carollo et al. 2013; Cassata et al. 2013; Krogager et al. 2013). The formation path of these extreme systems is largely unknown. Simulations indicate that highly dissipational interactions on short timescales provide plausible mechanisms for creating compact stellar populations, through either major mergers (e.g., Naab et al. 2007, 2009) or dynamical instabilities fed by cold gas accretion (Dekel et al. 2009). A possible scenario is major gas-rich mergers at high redshift (Wuyts et al. 2010) in which the gas is driven to the center, igniting a massive nuclear starburst followed by an active galactic nucleus (AGN)/QSO phase that quenches the star formation and leaves behind a compact remnant (Sanders et al. 1988; Hopkins et al. 2006; Wuyts et al. 2010). This is consistent with local stellar archaeology studies that imply that massive ellipticals must have short formation timescales of less than 1 Gyr (e.g., Thomas et al. 2005).

[18] FWO Pegasus Marie Curie Fellow.

Several authors have pointed out that submillimeter galaxies (SMGs) may be examples of the above scenario (e.g., Blain et al. 2004; Chapman et al. 2005; Tacconi et al. 2006, 2008; Toft et al. 2007; Cimatti et al. 2008; Capak et al. 2008; Schinnerer et al. 2008; Coppin et al. 2008; Michałowski et al. 2010a; Smolčić et al. 2011; Ricciardelli et al. 2010), but see Riechers (2013) for a counterexample. The SMG population is dominated by galaxies undergoing intense, dust-enshrouded starbursts. A large fraction of SMGs with measured CO profiles show double-peaked profiles, evident of ongoing major mergers or rotation (Frayer et al. 1999; Neri et al. 2003; Sheth et al. 2004; Kneib et al. 2005; Greve et al. 2005; Tacconi et al. 2006; Riechers et al. 2011b; Ivison et al. 2013; Fu et al. 2013). The autocorrelation length of SMGs is similar to that of optically selected QSOs, suggesting that SMGs and QSOs live in similar mass haloes and that the ignition of a QSO could be the event that quenches the star formation in SMGs (Hickox et al. 2012). This is consistent with observations suggesting that the hosts of the most luminous QSOs, i.e., those likely associated with the formation of massive quiescent galaxies, are found to be primarily major mergers (Treister et al. 2012; Riechers et al. 2008), a result that is corroborated by Olsen et al. (2013), who find that luminous AGNs in massive $z \sim 2$ galaxies must be triggered by external processes. Interestingly, Olsen et al. (2013) also find evidence for low-luminosity AGNs in the vast majority of massive quiescent galaxies at $z \sim 2$, suggesting that AGNs play active roles in the quenching of their star formation. The correlation length of SMGs is similar to that of $z \sim 2$ galaxies with $M_* > 5 \times 10^{10} M_\odot$ ($r_0 = 7.66 \pm 0.78$), while $z \sim 2$ galaxies with $M_* > 10^{11} M_\odot$ cluster more strongly ($r_0 = 11.49 \pm 1.26$; Wake et al. 2011).

Recent advances in near-infrared (NIR) spectroscopy have made it possible for the first time to accurately constrain the age, dust content, and past star formation history of the brightest $z \sim 2$ quiescent galaxies through absorption line diagnostics and spectral fitting in the rest-frame optical (Kriek et al. 2009; Onodera et al. 2010, 2012; van de Sande et al. 2011, 2012; Toft et al. 2012). These galaxies have spectra typical of poststarburst galaxies, with no detected emission lines. However, they have strong Balmer absorption lines, which suggests that they underwent major starbursts that were quenched 1–2 Gyr prior to the time of observation (i.e., at $3 < z < 6$). Several of these galaxies show evidence of significant dust abundance (with A_V values up to ~ 1 mag), and they are baryon dominated, as is the case for local poststarburst galaxies (Toft et al. 2012). In combination with their extremely compact stellar populations, these observations suggest that the majority of the stars in $z \sim 2$ quiescent galaxies formed in intense, possibly dust-enshrouded nuclear starbursts, a scenario very similar to what is observed in $z \sim 2$ SMGs.

Velocity dispersions of $z \sim 2$ quiescent galaxies measured from the width of absorption lines are in the range of 300–500 km s^{-1} (e.g., Toft et al. 2012; van de Sande et al. 2012), which is significantly higher than what is found in local ellipticals of similar stellar mass but comparable to the FWHM of molecular lines in $2 < z < 3$ SMGs (in the range of 350–800 km s^{-1}, with a mean equivalent rotational velocity of $\langle v_c \rangle = 392 \pm 134$ km s^{-1}; Tacconi et al. 2006). The line-emitting gas of SMGs, as traced by high-J CO lines, is found to be spatially very compact, with a mean size of $\langle R_e \rangle = 2.0 \pm 0.3$ kpc (Tacconi et al. 2006), which is comparable to the mean spatial extent $\langle R_e \rangle = 1.96 \pm 0.8$ kpc of the stellar populations in the quiescent $z \sim 2$ galaxies (Krogager

et al. 2013). We note, however, that studies of lower-J CO lines suggest that some SMGs may have more extended CO disks (Ivison et al. 2011; Riechers et al. 2011c). The median dynamical mass measured from CO(1–0) for $z \sim 2$ SMGs, $\langle M_{\rm dyn} \rangle = (2.3 \pm 1.4) \times 10^{11} M_\odot$ (Ivison et al. 2011), is similar to that measured for $z \sim 2$ quiescent galaxies, $\langle M_{\rm dyn} \rangle = (2.5 \pm 1.3) \times 10^{11} M_\odot$ (Toft et al. 2012).

Despite the many similarities between SMGs and $z \sim 2$ quiescent galaxies, a major obstacle in establishing an evolutionary link between the two galaxy types is their similar redshift distribution. While the quiescent nature and derived ages for $z \sim 2$ quiescent galaxies suggest they formed at $z \gtrsim 3$, the peak of the known SMG population was until recently found to be at $z \sim 2$, with very few examples known at $z \gtrsim 3$ (e.g., Chapman et al. 2005), a fact that renders an evolutionary link between the two populations unlikely. Recently, however, improved selection techniques have uncovered a substantial tail stretching out to redshifts of $z \sim 6$ (Capak et al. 2008; Schinnerer et al. 2008; Daddi et al. 2009a, 2009b; Knudsen et al. 2010; Carilli et al. 2010, 2011; Riechers et al. 2010, 2013; Cox et al. 2011; Combes et al. 2012; Yun et al. 2012; Smolčić et al. 2012a; Michałowski et al. 2012b; Hodge et al. 2012, 2013a).

In this article we present evidence for a direct evolutionary link between the two extreme galaxy populations by comparing the properties of two unique samples in the COSMOS field: (1) a spectroscopically confirmed, representative sample of compact $z \sim 2$ quiescent galaxies with high-resolution *Hubble Space Telescope* (*HST*)/WFC3 imaging, and (2) a statistical sample of $z \gtrsim 3$ SMGs. In Section 2 we introduce the samples, and in Section 3 we present our results. In particular, in Section 3.1 we show that the distribution of formation redshifts for the $z \sim 2$ galaxies is similar to the observed redshift distribution of $z \gtrsim 3$ SMGs, and in Section 3.2 we compare the comoving number densities of the two populations. In Section 3.3 we derive structural properties of the $z \gtrsim 3$ SMGs, and in Section 3.4 we show that their stellar mass–size relation is similar to that of $z \sim 2$ quiescent galaxies. In Sections 3.5 and 3.6 we show that the duty cycle of the $z > 3$ SMG starbursts (which are derived assuming they are progenitors of $z \sim 2$ quiescent galaxies) is consistent with independent estimates and with the formation timescale derived for $z \sim 2$ quiescent galaxies (assuming they formed in Eddington-limited starbursts). In Section 4 we summarize and discuss the results.

Throughout this article we assume a standard flat universe with $\Omega_\lambda = 0.73$, $\Omega_m = 0.27$, and $H_0 = 71$ km s^{-1} Mpc^{-3}. All stellar masses are derived assuming a Chabrier (2003) initial mass function (IMF).

2. SAMPLES

2.1. Sample of $z \gtrsim 3$ SMGs

Based on dedicated follow-up studies with sub-mm interferometers (PdBI, SMA, CARMA) and optical/mm spectroscopy (with Keck/DEIMOS, EVLA, PdBI) toward 1.1 mm- and 870 μm-selected sources in the COSMOS field, Smolčić et al. (2012a) presented the redshift distribution of SMGs. This sample shows a tail of $z \gtrsim 3$ SMGs, corresponding to a significantly larger number density at these high redshifts than found in previous surveys (e.g., Chapman et al. 2005; Wardlow et al. 2011; Yun et al. 2012; Michałowski et al. 2012b). A possible reason for the difference is that previous surveys did not have (sub-)mm follow-up interferometry and therefore may be subject to identification biases. For example, Hodge et al.

Table 1
Sample of $z > 3$ Submillimeter Galaxies in COSMOS

	z	$r_{e,\mathrm{NIR}}$ (kpc)	Note	$r_{e,\mathrm{FIR}}$ (kpc)
AzTEC 1	4.64[a]	<2.6	Unresolved	$1.3 - 2.7$[c]
AzTEC 3	5.299[a]	<2.4	Unresolved	$<3 \pm 2$[d]
AzTEC 4	$4.93^{+0.43}_{-1.11}$	<2.5	Unresolved	...
AzTEC 5	3.971[a]	0.5 ± 0.4	*HST*/WFC3	...
AzTEC 8	3.179[a]	<3.0	Unresolved	...
AzTEC 10	$2.79^{+1.86}_{-1.29}$	0.7 ± 0.1	...	...
AzTEC 11-S	>2.58[b]	...	Not detected	...
AzTEC 13	>3.59[b]	...	Not detected	...
AzTEC 14-E	>3.03[b]	...	Not detected	...
AzTEC 15	$3.17^{+0.29}_{-0.37}$	5.0 ± 0.8	Very faint	...
J1000+0234	4.542[a]	3.7 ± 0.2	...	...
Vd-17871	4.622[a]	1.3 ± 0.4	...	...
GISMO-AK03	4.757[a]	1.6 ± 0.6	*HST*/WFC3	...

Notes. The top 11 galaxies constitute the S/N-limited, relatively complete statistical sample we use for estimating the comoving number density. The bottom two are spectroscopically confirmed $z > 3$ galaxies that we add to the sample for structural analysis only. We refer to Smolčić et al. (2012a) for details about the sample. The listed effective radii reported are circularized, i.e., $r_{e,c} = r_{e,m}\sqrt{b/a}$, where $r_{e,m}$ is the effective radius along the major axis and b/a is the axis ratio. $r_{e,\mathrm{FIR}}$ [kpc] are rest-frame FIR sizes from the literature, measured from high-resolution mm observations. For easy comparison to the NIR effective radii, we here quote Gaussian HWHMs.
[a] Spectroscopic redshift.
[b] mm-to-radio flux ratio based redshift.
[c] Younger et al. (2008).
[d] Riechers et al. (2010).

(2013b) show that many of the galaxies in the Wardlow et al. (2011) sample break up into multiple sources when studied at high resolution, which inevitably lead to misidentifications for some of the sources.

Here we use the Smolčić et al. (2012a) sample to estimate the comoving number density and other properties of $z \gtrsim 3$ SMGs. Our starting point is a 1.1 mm-selected sample, drawn from the AzTEC/JCMT 0.15 deg^2 survey of the COSMOS field (Scott et al. 2008) and observed with the Submillimeter Array (SMA) at 890 μm and $\sim 2''$ angular resolution in order to unambiguously associate multiwavelength counterparts (Younger et al. 2007, 2009). The 17 SMGs identified by the SMA follow-up form a statistical sample as they are drawn from a signal-to-noise limited (S/N$_{1.1\,\mathrm{mm}} > 4.5$), and flux-limited ($F_{1.1\,\mathrm{mm}} \gtrsim 4.2$ mJy), 1.1 mm-selected sample; they are also drawn over a contiguous area of 0.15 square degrees. We include one more SMG in this sample, J1000+0234 ($F_{1.1\,\mathrm{mm}} = 4.8 \pm 1.5$ mJy, S/N$_{1.1\,\mathrm{mm}} \sim 3$), which is confirmed to be at $z = 4.542$ (Capak et al. 2008; Schinnerer et al. 2008, 2009). Nine out of these 18 interferometrically detected galaxies have spectroscopic redshifts (4 are confirmed to be at $z \gtrsim 3$; Capak 2009; Capak et al. 2010; Schinnerer et al. 2009; Riechers et al. 2010; A. Karim et al., in preparation), while for the remainder precise photometric redshifts ($\sigma_{\Delta z/(1+z_{\mathrm{spec}})} = 0.09$) were computed by Smolčić et al. (2012a). The $z \gtrsim 3$ SMGs from this sample are listed in Table 1. The top 11 objects constitute our statistical sample. We will use these in the following sections to estimate the redshift distribution and comoving number density of $z \gtrsim 3$ SMGs. The bottom two objects are additional spectroscopically confirmed $z \gtrsim 3$ SMGs in the COSMOS field, which we add to the sample for structural analysis only.

The flux-limited sub-mm selection ensures a relatively homogeneous sample of the most intensely star-forming dust-obscured galaxies at $z \gtrsim 3$: Due to the negative k-correction, the sub-mm flux detection limit corresponds roughly to a cut in star formation rate (SFR) over the considered redshift range. Note that while a fraction of single-dish-detected SMGs break up into multiple components when studied with interferometry at $\leqslant 2''$ resolution, this is only the case for two of the galaxies studied here (AzTEC 11 and 14). In the present study we assume that the close individual components are related and count them as one in the number density calculations (thus assuming they will eventually merge into one galaxy). As the galaxies are not resolved in the MIR-mm photometry, derived properties (infrared luminosities, SFRs, dust masses, etc.) pertain to the combined system. Neither of the two galaxies are detected in the optical-NIR; thus, derived sizes and stellar masses for the sample are not affected.

2.2. Far-infrared Emission of the $z \gtrsim 3$ SMGs

In order to directly constrain the SFRs, dust, and gas masses of the $z \gtrsim 3$ SMGs, we made use of the (sub)-mm (AzTEC, LABOCA, MAMBO, SMA, CARMA, and PdBI) and far-infrared (FIR) (*Spitzer* MIPS, *Herschel* PACS, and SPIRE) observations of the COSMOS field (Sanders et al. 2007; Lutz et al. 2011; Oliver et al. 2012; Scott et al. 2008; Aretxaga et al. 2011; Bertoldi et al. 2007; Younger et al. 2007, 2008; Smolčić et al. 2012a, 2012b). The *Herschel* data consist of deep PACS 100 and 160 μm observations, taken as part of the PACS Evolutionary Probe (PEP; Lutz et al. 2011) guaranteed time key programme and SPIRE 250, 350, and 500 μm observations taken as part of the Herschel Multitiered Extragalactic Survey (HerMES;[19] Oliver et al. 2012).

PACS and SPIRE flux densities were measured using a point-spread function (PSF) fitting analysis (Magnelli et al. 2009; Roseboom et al. 2010), guided by the position of sources detected in the deep COSMOS 24 μm observations from the Multiband Imaging Photometer (MIPS; Rieke et al. 2004) on board the *Spitzer Space Observatory* ($3\sigma \sim 45\,\mu$Jy; Le Floc'h et al. 2009). We cross-matched our $z > 3$ SMG sample with this MIPS-PACS-SPIRE catalogue using a matching radius of $2''$. Results of these matches were all visually checked. For $z > 3$ SMGs not included in the MIPS-PACS-SPIRE catalogue because of a lack of MIPS counterpart, we compute their PACS and SPIRE flux densities using a PSF-fitting analysis guided by their positions. Further details of the FIR photometry are presented in V. Smolčić et al. (in preparation).

Among the 13 $z \gtrsim 3$ SMGs, 9 have secure mid-/far-infrared detections, 2 have tentative mid-/far-infrared detections, and 2 are undetected at infrared wavelengths. From the FIR–mm spectral energy distribution (SED) of the $z \gtrsim 3$ SMGs, we infer their infrared luminosities and dust masses using the dust model of Draine & Li (2007, hereafter DL07) as described in detail in Magnelli et al. (2012). The infrared luminosity (L_{IR}) is derived by integrating the best-fitting normalized SED templates from the DL07 library from rest-frame 8 to 1000 μm. From these we can accurately estimate the star formation activity of the $z \gtrsim 3$ SMGs, using the standard L_{IR}-to-SFR conversion of Kennicutt (1998), assuming a Chabrier IMF:

$$\mathrm{SFR}\,[M_\odot\,\mathrm{yr}^{-1}] = 10^{-10}\,L_{\mathrm{IR}}\,[L_\odot]. \qquad (1)$$

---

[19] http://hermes.sussex.ac.uk

Table 2
Far-infrared SED Properties of the $z \gtrsim 3$ SMG Sample

	$\log(M_\star)$[a] $(M_\odot)$	$q_{\rm PAH}$[b]	γ[b]	$U_{\min}$[b]	$\log(M_{\rm dust})$[b] $[M_\odot]$	$\log(L_{\rm IR})$[c] $[L_\odot]$	SFR[b,e] $(M_\odot\ {\rm yr}^{-1})$	$\log(M_{\rm gas})$[c] $(M_\odot)$	FIR Detection[d]	$\log(M_{\rm gas})_{\rm CO}$[f] $(M_\odot)$
AzTEC 1	$10.9^{+0.1}_{-0.1}$	0.47%	0.070	25.0	9.1 ± 0.1	13.36 ± 0.09	2291 ± 528	11.7 ± 0.1	Secure	
AzTEC 3	$11.2^{+0.1}_{-0.1}$	0.47%	0.290	25.0	9.3 ± 0.1	13.37 ± 0.04	2344 ± 226	11.3 ± 0.1	Secure	10.7
AzTEC 4	$11.2^{+0.1}_{-0.1}$	4.58%	0.080	25.0	9.6 ± 0.2	13.25 ± 0.15	1778 ± 733	11.6 ± 0.2	Tentative	
AzTEC 5	$10.9^{+0.5}_{-0.5}$	0.47%	0.190	25.0	9.4 ± 0.1	13.43 ± 0.02	2692 ± 127	11.4 ± 0.1	Secure	
AzTEC 8	$11.5^{+0.1}_{-0.1}$	0.47%	0.090	25.0	9.7 ± 0.1	13.45 ± 0.01	2818 ± 66	11.7 ± 0.1	Secure	
AzTEC 10	$10.5^{+0.1}_{-0.1}$	2.50%	0.060	5.00	9.6 ± 0.1	12.58 ± 0.10	380 ± 98	11.8 ± 0.1	Secure	
AzTEC 11-S	$\ldots$	0.47%	0.040	25.0	9.6 ± 0.1	13.30 ± 0.01	1995 ± 46	$\ldots$	Secure	
AzTEC 13	$\ldots$	4.58%	0.160	2.00	9.9 ± 0.3	12.70 ± 0.20	501 ± 293	$\ldots$	Upper limits	
AzTEC 14-E	$\ldots$	0.47%	0.290	0.70	9.8 ± 0.2	12.48 ± 0.18	302 ± 155	$\ldots$	Upper limits	
AzTEC 15	$11.2^{+0.1}_{-0.1}$	3.19%	0.010	20.0	9.3 ± 0.1	12.73 ± 0.08	537 ± 108	11.4 ± 0.1	Secure	
J1000+0234	$10.9^{+0.1}_{-0.1}$	1.77%	0.150	25.0	9.3 ± 0.1	13.17 ± 0.09	575 ± 275	11.8 ± 0.4	Tentative	10.4
Vd-17871	$10.9^{+0.1}_{-0.1}$	4.58%	0.250	25.0	9.1 ± 0.1	13.09 ± 0.06	1230 ± 182	11.2 ± 0.2	Secure	
GISMO-AK03	$12.1^{+0.1}_{-0.1}$	4.58%	0.290	3.00	9.5 ± 0.2	12.66 ± 0.19	457 ± 250	11.5 ± 0.2	Secure	

Notes.
[a] Derived using MAGPHYS from the optical-FIR SED. The errors are the formal errors associated with the fit and do not include systematic errors, which can be up to ± 0.5 dex; see Section 2.3.
[b] The DL07 model describes the interstellar dust as a mixture of carbonaceous and amorphous silicate grains. Here we list the best-fitting values of its four free parameters: (1) $q_{\rm PAH}$, which controls the fraction of dust mass in the form of polycyclic aromatic hydrocarbon (PAH) grains. (2) γ, which controls the fraction of dust mass exposed to a power-law ($\alpha = 2$) radiation field ranging from $U_{\min}$ to $U_{\max}$; the rest of the dust mass (i.e., $1 - \gamma$) being exposed to a radiation field with a constant intensity $U_{\min}$. (3) $U_{\min}$, which controls the minimum radiation field seen by the dust ($U_{\max}$ is fixed to a value of 10^6). (4) $M_{\rm dust}$, which controls the normalization of the SED.
[c] Quantities derived from the best-fitting DL07 models (see Section 2.2).
[d] "Secure": The source is relatively isolated and detected at S/N > 3. "Tentative": The source is detected at S/N > 3, but the flux density estimates may be affected by bright closeby objects. "Upper limit": The source is not detected at S/N > 3.
[e] SFRs are notoriously model dependent, e.g., from a detailed analysis of all available data for AzTEC-3, and assuming a top-heavy IMF, Dwek et al. (2011) found a significantly lower SFR than derived here from the DL07 fits.
[f] Gas masses derived from CO observations (Schinnerer et al. 2008; Riechers et al. 2010).

Finally, we estimate the gas masses of the sample through $\log(M_{\rm gas}/M_{\rm dust}) = -0.85 * Z + 9.4$ (Leroy et al. 2011), where $Z = 2.18 \times \log(M_\star) - 0.0896 * \log(M_\star)^2 - 4.51$ (Erb et al. 2006; Genzel et al. 2012).[20] This method has been used successfully in the local universe (e.g., Leroy et al. 2011; Bolatto et al. 2011), as well as at high redshift (Magdis et al. 2011, 2012; Magnelli et al. 2012). Assumptions and limitations of this method in the case of high-redshift galaxies are extensively discussed in Magnelli et al. (2012). Results of the FIR SED fits and derived quantities are summarized in Table 2 and used in the following analysis to establish an evolutionary link between $z \gtrsim 3$ SMGs and quiescent $z \sim 2$ galaxies. The derived gas masses are comparable to or larger than the derived stellar masses: $\langle f_g \rangle = \langle M_{\rm gas}/(M_\star + M_{\rm gas}) \rangle = 0.71 \pm 0.03$, in agreement with the high gas fractions found in previous studies of high-redshift SMGs (e.g., Carilli et al. 2010; Riechers et al. 2011c). We caution, however, that gas masses estimated from FIR SED fits are relatively uncertain (potentially up to a factor of 5–10). For example, in Table 2 we list gas masses for two objects in our sample that have independent estimates derived from CO line emission. These are significantly different from our SED estimates. The main factors contributing to the uncertainties in the SED estimates are that the sub-mm measurements do not trace cold gas very well, in which case the (sub)-mm/CO flux ratio is much lower than in the starburst nucleus but

where a lot of the gas mass may reside. The other factors are the metallicity correction (which has a large scatter) and the assumption about the gas-to-dust ratio. The main factors contributing to the uncertainty of the CO measurements are the assumed $\alpha_{\rm CO}$, which can be uncertain by a factor >2, and the excitation corrections, which can be uncertain by a factor of ~2–4.

2.3. Stellar Mass Estimates for the $z \gtrsim 3$ SMGs

We estimate stellar masses of the $z \gtrsim 3$ SMGs from their UV–MIR ($8\,\mu{\rm m}$) broadband photometry as described in V. Smolčić et al. (in preparation). Briefly, stellar masses were derived by fitting the observed broadband UV–MIR SEDs with the MAGPHYS code (da Cunha et al. 2008). The stellar component in the MAGPHYS models is based on Bruzual & Charlot (2003) stellar population synthesis models assuming various star formation histories (exponentially declining SFHs (with random timescales) + superimposed stochastic bursts) and a Chabrier (2003) IMF. The stellar masses for the SMGs and their formal uncertainties drawn from the probability distribution function (generated from the χ^2 fit values by MAGPHYS) are given in Table 2. We note, however, that stellar masses for SMGs are strongly dependent on the assumed star formation histories and may lead to systematic discrepancies of ± 0.5 dex given different assumptions and stellar population synthesis models (see Table 1 in Michałowski et al. 2012a) and whether or not emission lines are included in the templates (Schaerer et al. 2013). For example, using the double SFHs implemented in GRASIL (Silva et al. 1998; Iglesias-Páramo et al. 2007), we find

---

[20] Thus making the assumption that the mass–metallicity relation at $z \sim 2$ applies to galaxies at $z > 3$.

systematically higher stellar masses, consistent with the results from Michałowski et al. (2010b). On the other hand, dynamical mass considerations based on CO line observations for two objects in our sample (Schinnerer et al. 2008; Riechers et al. 2010) suggest lower stellar masses than inferred by MAGPHYS. Therefore, here we adopt the middle values, i.e., the stellar masses computed by MAGPHYS+BC03, noting that these may be subject to systematic uncertainties.

2.4. Sample of z ~ 2 Compact Quiescent Galaxies

It is well established from deep multiwaveband photometric surveys that a substantial population of quiescent massive galaxies with extremely compact structure exists at $z \sim 2$ (Daddi et al. 2005; Toft et al. 2005, 2007, 2009; Trujillo et al. 2006; Franx et al. 2008; Williams et al. 2010; van Dokkum et al. 2010; Brammer et al. 2011; Szomoru et al. 2011, 2012; Damjanov et al. 2011; Newman et al. 2012; Cassata et al. 2013). Samples of spectroscopically confirmed, $z \sim 2$ quiescent galaxies with accurate stellar population model fits and high angular resolution space-based NIR imaging are much more sparse (van Dokkum et al. 2008). As a high-quality comparison set to the $z > 3$ SMGs we use the sample of Krogager et al. (2013, K13 hereafter). This sample consists of 16 spectroscopically confirmed massive quiescent galaxies, selected from the 3DHST survey in the COSMOS field by requiring strong 4000 Å breaks in the grism observations. As shown in K13, this effectively selects a representative sample of massive ($\log M > 10.9$) quiescent galaxies around $z \sim 2$. The high S/N grism spectra around the break in combination with multiwaveband photometry from the COSMOS survey allows for strong constraints on the stellar populations including stellar masses, dust contents, mean stellar ages, i.e, the time elapsed since the last major episode of star formation, as well as formation redshifts (derived from the stellar ages). The sample is also covered by high-resolution NIR imaging with *HST*/WFC3 from the CANDELS survey (Grogin et al. 2011; Koekemoer et al. 2011), yielding accurate constraints on the rest-frame optical surface brightness profiles and effective radii (r_e).

3. RESULTS

3.1. Redshift Distributions

From the spectroscopic redshifts and mean stellar ages available for the quiescent $z \sim 2$ galaxy sample described in Section 2.4 we can estimate the distribution of their formation redshifts. In Figure 1 this distribution is compared to the observed redshift distribution of the sample of $z \gtrsim 3$ SMGs described in Section 2.1. Due to the small number of galaxies in both samples, a one-to-one correspondence is not expected. However, we stress that the two distributions are similar, with a peak at $z \sim 3$ and a tail toward higher redshifts. A two-sample Kolmogorov–Smirnov (K-S) test yields a statistic of 0.29 with a p-value of 54%, and it is thus not inconsistent with the two redshift distributions being drawn from the same parent distribution.

3.2. Comoving Number Densities

The next step in establishing an evolutionary connection between $z \gtrsim 3$ SMGs and quiescent galaxies at $z \sim 2$ is to compare their comoving number densities. The comoving number density of massive quiescent galaxies as a function of redshift is well constrained from photometric redshift and stellar population
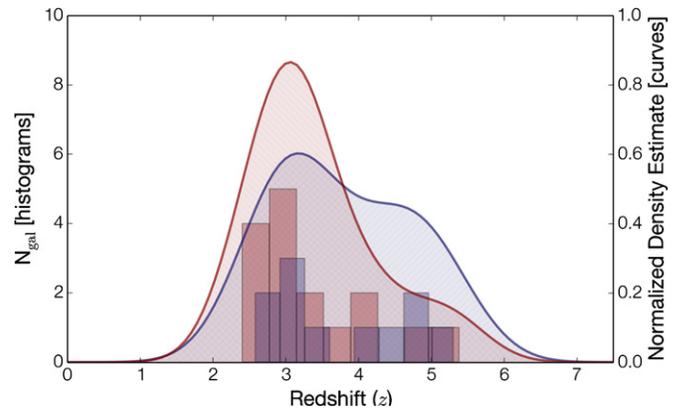

Figure 1. Comparison of the redshift distribution of $z > 3$ SMGs and the formation redshifts of $z \sim 2$ quiescent galaxies. The red histogram shows the distribution of formation redshifts estimated for a spectroscopically confirmed sample of compact quiescent galaxies at $z \sim 2$ from their observed redshift and derived luminosity-weighted ages of their stellar populations (K13). The blue histogram shows the distribution of redshifts of the statistical sample of $z > 3$ SMGs. Note that the galaxies that only have lower limits on the redshifts have been placed in the bins corresponding to those limits, and that the histogram includes two galaxies where the best-fitting redshift is slightly below 3, but for which a $z > 3$ photometric redshift solution falls within the 99% confidence interval. The smooth curves show probability density distributions (kernel density estimates (KDEs)) of the two populations. The two redshift distributions are similar, consistent with the hypothesis that $z > 3$ SMGs are the direct progenitors of $z \sim 2$ compact quiescent galaxies (cQGs).

(A color version of this figure is available in the online journal.)

model fits to deep multiwaveband photometry (e.g., Williams et al. 2010; Brammer et al. 2011). Here we estimate a comoving number density of $(6.0 \pm 2.1) \times 10^{-5}$ Mpc^{-3} for quiescent galaxies at $z \sim 2$ with $\log(M/M_\odot) > 11$ as the mean of the densities measured at $z = 1.9$ and $z = 2.1$ by Brammer et al. (2011). The error includes a contribution of cosmic variance of 12% (Moster et al. 2011).

To derive the surface number density of $z \gtrsim 3$ SMGs, we take all SMGs from the 1.1 mm-selected COSMOS sample that could lie at $z \gtrsim 3$ given their lower or upper 99% confidence levels of the photometric redshift (reported in Table 4 in Smolčić et al. 2012a). We then derive an average value of the surface density by taking the most probable photometric redshift (or spectroscopic redshift where available),[21] and the lower[22] and upper[23] surface density values by taking the limiting redshifts corresponding to the 99% confidence intervals of the photometric redshifts. This yields a surface density of $z \gtrsim 3$, bright ($F_{1.1\,mm} \gtrsim 4.2$ mJy) SMGs of 60 ± 10 deg^{-2}. Note that conservatively excluding from the analysis all three SMGs in the sample that are not significantly detected at other wavelengths (AzTEC11S, AzTEC13, AzTEC14E), and thus only have lower redshift limits, yields a surface density of 40 deg^{-2}.

The derived surface density values for $z \gtrsim 3$ SMGs may be subject to systematic effects. The completeness of the AzTEC/ JCMT COSMOS survey, shown in Figure 8 in Scott et al. (2008), is roughly 50%, 70%, and 90% at $F_{1.1\,mm} = 4.2$, 5, and 6 mJy, respectively. Taking this into account in combination with the deboosted 1.1 mm fluxes of the SMGs (see Younger et al. 2007,

---

[21] Taking the most probable photometric redshift reveals that nine SMGs (AzTEC1, AzTEC3, AzTEC4, AzTEC5, AzTEC8, AzTEC13, AzTEC14E, AzTEC15, and J1000+0234) are at $z > 3$.
[22] In this case eight SMGs (AzTEC1, AzTEC3, AzTEC4, AzTEC5, AzTEC8, AzTEC13, AzTEC14E, and J1000+0234) are at $z > 3$.
[23] In this case 10 SMGs (AzTEC1, AzTEC3, AzTEC4, AzTEC5, AzTEC8, AzTEC10, AzTEC11S, AzTEC13, AzTEC14E, and J1000+0234) are at $z > 3$.
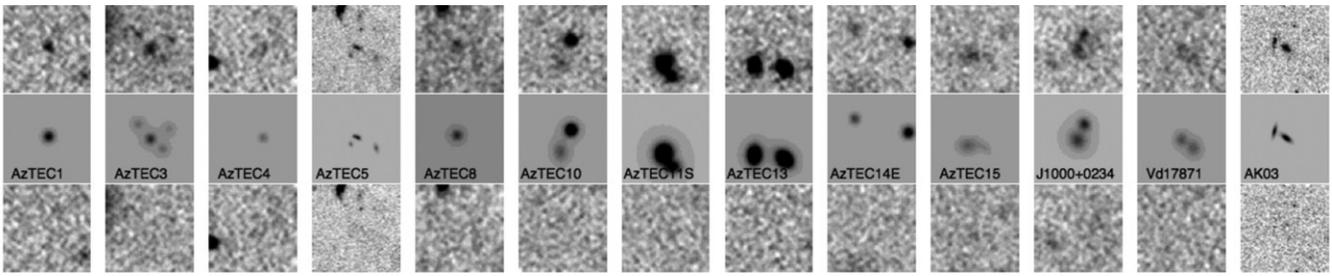
Figure 2. Gallery of $z > 3$ SMGs. Top: NIR images, $8''$ on a side. For AzTEC5 and GISMO-AK03 we show *HST*/WFC3 F160W images from the CANDELS survey. For the rest we show stacked *Y*-, *J*-, *H*-, and *K*-band images from the UltraVISTA survey. Middle: Sersic $n = 1$ GALFIT models of the 2D surface brightness distributions of the SMGs and their nearby companions. Bottom: Residual images, i.e., the original images shown in the top panel, subtracted the best-fitting models in the middle panel.

2009) reveals that the derived surface densities could be roughly a factor of 1.5 higher than that reported above. On the other hand, the AzTEC/JCMT COSMOS field may be overdense (Austermann et al. 2009), which would imply that the true $z \gtrsim 3$ SMG surface density averaged over a larger area would be lower.

Our best estimate of the comoving number density of $3 < z < 6$ SMGs is $(2.1 \pm 0.4) \times 10^{-6}$ Mpc^{-3}, which is significantly lower than the space density of $z \sim 2$ quiescent galaxies. This is expected as $z \gtrsim 3$ galaxies only enter the mm-selection criterion during their intense starburst phase. In Section 3.5 we use the observed difference in comoving number densities to constrain the duty cycle of the SMG starbursts.

3.3. Rest-frame UV–Optical Structure of $z > 3$ SMGs: Disks, Spheroids, or Mergers?

The high redshifts and large amounts of dust in the $z \gtrsim 3$ SMGs render them extremely faint in the rest-frame UV and optical, despite their high stellar masses and SFRs. This makes it challenging to constrain their structure. To achieve the least biased estimates of the distribution of stellar mass, one would need to study the surface brightness distributions in the rest-frame optical/NIR, or as close to these wavebands as possible. Ideally, the observations would be done in the observed mid-infrared, but at the low spatial resolution of current facilities (e.g., *Spitzer*) the galaxies remain unresolved. Until *James Webb Space Telescope* becomes operational, the best that can be achieved is to study the galaxies in the observed NIR. For most of the galaxies in the sample this wavelength range probes rest-frame wavelengths around the 4000 Å break and thus should be a relatively good tracer of the stellar mass distribution. For two galaxies (AzTEC5 and GISMO-AK03), we use space-based NIR imaging with *HST*/WFC3, which is available from the CANDELS survey. This is preferable to ground-based imaging given the higher resolution (FWHM $\sim 0''.2$). For the remaining galaxies we use deep NIR imaging provided by the UltraVista survey (5σ AB depths range from 23.7 in the *K* band to 24.6 in the *Y* band; McCracken et al. 2012). The resolution of these observations is lower (FWHM $\sim 0''.8$), but it has been demonstrated that relatively unbiased sizes (down to a fraction of the FWHM$_{PSF}$) can be derived from such data when the S/N is high and the PSF is well known (e.g., Trujillo et al. 2006; Toft et al. 2009; Williams et al. 2010). To increase the S/N, we stack the *Y*-, *J*-, *H*-, and *K*-band images.

Postage stamp images of the galaxies are shown in the top panel of Figure 2. NIR counterparts of 10 of the 13 sources are detected, 8 of which have relatively high S/N (the faintest ones have S/N ~ 10). We fit 2D Sersic models to their surface brightness distributions with GALFIT (Peng et al. 2002), using

similarly stacked images of nearby stars as PSF models. We find the Sersic n to be relatively poorly constrained from the data. Leaving it free in the fits in all cases results in low values $n < 2$, with a median value of $\langle n \rangle = 0.6 \pm 0.1$, but with relatively large errors. To limit the degrees of freedom in the fits, we therefore fix it to $n = 1$. The reduced χ^2 of these fits are in all cases similar to those with n free, and they are better than fits with n fixed to 4.

The best-fitting effective radii, encompassing half the light of the model, are reported in Table 1. Half of the detected galaxies (five) have close companions. In these cases we model both components simultaneously and report the parameters for the main component (closest to the center of the mm emission). Also listed in Table 1 are rest-frame FIR sizes for two galaxies in our sample derived from interferometric sub-mm imaging observations. These agree with the sizes derived from the NIR data. The rest-frame FIR sizes directly measure the extent of the star-forming regions, which we hypothesize evolves into the compact stellar populations at $z = 2$; thus, the agreement is encouraging.

Our analysis shows that apart from being very compact, the $z > 3$ SMGs are not isolated, smooth, single-component galaxies. All the detected galaxies show evidence of close companions or clumpy substructure (see Figure 2). From these observations alone, it is not possible to deduce whether this is due to chance projections, ongoing minor/major mergers, or perhaps multiple star-forming regions in individual galaxies, as resolved photometry and spectroscopy are not available. We note, however, that the two galaxies with *HST*/WFC3 data appear to have well-separated individual components of comparable brightness, favoring the merger interpretation. This is consistent with direct observational evidence for SMGs being major mergers, i.e., having multiple close components at the same redshift (e.g., Fu et al. 2013; Ivison et al. 2013). Simulations suggest that the timescale for major mergers is typically 0.39 ± 0.30 Gyr (Lotz et al. 2010). The cosmic time available between the observed epoch of the SMGs at $z = 3$–6 and their proposed remnants at $z = 2$ is 1–2 Gyr. If (some of) the SMGs are major mergers, there is thus sufficient time available for them to coalesce to a single quiescent remnant at $z = 2$.

In the local universe most star-forming galaxies are well fit by exponential disk profiles corresponding to $n = 1$ (Wuyts et al. 2011), while irregular galaxies and (precoalescence) mergers are often best fit by models with lower n-values ($n < 1$). At the S/N and resolution of the galaxies in the Ultravista data the confidence in derived Sersic parameters is limited. However, the persisting low values found for the whole $z > 3$ SMG sample, including the two galaxies with the higher resolution *HST*/WFC3 data, suggest that the galaxies are more consistent with
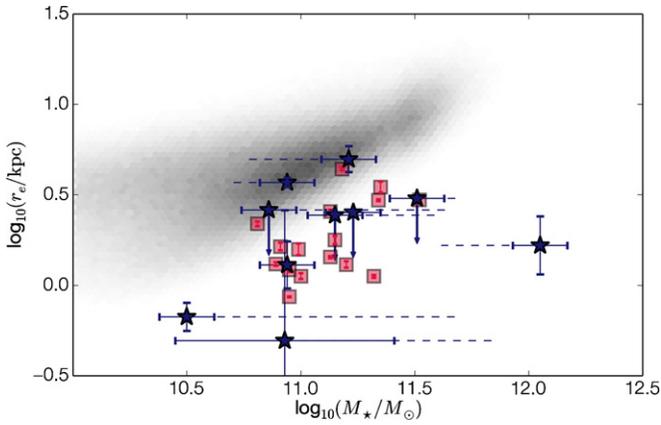
Figure 3. Comparison of the stellar mass–size plane of $z > 3$ SMGs, $z \sim 2$ quiescent galaxies, and local galaxies. The red points represent $z \sim 2$ quiescent galaxies. Black points represent $z > 3$ SMGs. For the latter, the solid error bars represent the errors associated with the MAGPHYS SED fits. The dotted error bars are possible systematic errors that extend to values that we derive using the Michałowski et al. (2010a) templates. The gray cloud shows the mass–size distribution of massive local galaxies in the Sloan Digital Sky Survey. The mass–size distribution of SMGs is similar to that of $z \sim 2$ quiescent galaxies, significantly offset from the local relation and consistent with a direct evolutionary connection between the two populations.

(A color version of this figure is available in the online journal.)

disks or mergers than spheroids. A similar conclusion was found for a sample of 22 SMGs at $1 < z < 3$ with *HST*/WFC3 data (Targett et al. 2013) for which the majority were best fit by low-n Sersic models, with a mean $\langle n \rangle = 1.2 \pm 0.1$. If $z > 3$ SMGs are progenitors of $z \sim 2$ quiescent galaxies, then their evolution must include a transformation of their surface brightness profiles that increase their Sersic indices, as surface brightness profiles of quiescent galaxies at $z \sim 2$ are more centrally concentrated (Wuyts et al. 2011; Szomoru et al. 2011; Bell et al. 2012), e.g., the sample of K13 has $\langle n \rangle = 4.0 \pm 0.1$. We discuss a possible mechanism for this transformation in Section 4.

3.4. Mass–Size Relation

Combining the derived stellar masses and effective radii of the $3 < z < 6$ SMGs, in Figure 3 we compare their stellar mass–size distribution to that of $z = 2$ quiescent galaxies and of massive early-type galaxies in the local universe. Two of the 10 NIR-detected SMGs are relatively extended with effective radii comparable to those in local galaxies of similar mass. Both of these (AzTEC 10 and AzTEC 15) appear from their NIR images to be ongoing mergers. The remaining 8 galaxies are extremely compact, with $r_e \lesssim 2.5$ kpc. Four are unresolved in the Ultravista data. For these we adopt upper limits on their effective radii corresponding to $0.5 \times \mathrm{FWHM}_{PSF}$.

The stellar mass–size distribution of the $3 < z < 6$ SMGs is similar to that of $z \sim 2$ quiescent galaxies. Both populations are smaller than local galaxies of similar mass by an average factor of ~ 3. From the derived quantities we can infer the mean internal stellar mass surface densities within the effective radius ($\Sigma = 0.5 \, M_\star / \pi r_e^2$) of the $z > 3$ SMGs and $z = 2$ cQGs, which we find to be similar: $\langle \log(\Sigma) \rangle_{SMGs} \sim 9.9 \pm 0.1 \, M_\odot \, \mathrm{kpc}^{-2}$, $\langle \log(\Sigma) \rangle_{cQGs} \sim 9.8 \pm 0.1 \, M_\odot \, \mathrm{kpc}^{-2}$, in both cases more than an order of magnitude higher than in local early-type galaxies of similar mass. This is consistent with a picture where the SMGs passively evolve into compact quiescent galaxies after their starbursts are quenched.

3.5. Duty Cycle of SMG Starbursts

The observed space density of $z \gtrsim 3$ SMGs is a factor of ~ 30 lower than the space density of $z \sim 2$ quiescent galaxies (see Section 3.2). However, the SMGs only enter the sub-mm-selected ($F_{1.1 \, mm} \gtrsim 4.2$ mJy) sample during their intense starburst phase where they have very high SFRs. The duration of this phase, i.e., the duty cycle t_{burst}, which ends when the supply of gas is depleted or the star formation is quenched, e.g., by feedback from supernovae or AGNs, has been estimated to be in the range of 40–200 Myr based on gas depletion timescales (Greve et al. 2005; Tacconi et al. 2006; Riechers et al. 2011a) and clustering analysis (Hickox et al. 2012). If we assume that all of the $z \gtrsim 3$ SMGs evolve into $z \sim 2$ quiescent galaxies, and that they only undergo one SMG phase, we can estimate the average duty cycle of their starbursts from the observed comoving number densities of the two populations as

$$t_{burst} = t_{obs} \times (n_{SMG, z \gtrsim 3} / n_{q, z=2}), \qquad (2)$$

where t_{obs} is the cosmic epoch corresponding to the redshift interval $3 < z < 6$ from which the $z \gtrsim 3$ SMGs are selected. Using the comoving number densities, we can thus constrain the duty cycle of the SMGs to $t_{burst} = 42^{+33}_{-15}$ Myr. This number, however, does not include possible systematic uncertainties on the number density of SMGs discussed in Section 3.2. If we conservatively assume the two extreme cases where (1) the SMG sample is 100% complete, and the field is three times overdense; and (2) the sample is a factor of 1.5 incomplete but not overdense, the derived timescales are in the range of $14 \, \mathrm{Myr} < t_{SMG} < 62 \, \mathrm{Myr}$. The systematic uncertainty on the timescale is thus of the order of 24 Myr. Therefore, our constraints on the average duty cycle in $z \gtrsim 3$ SMGs is $t_{burst} = 42^{+40}_{-29}$ Myr, where the errors have been added in quadrature. This value is consistent with the independently estimated duty cycles based on gas depletion timescales, thus affirming the idea that $z \gtrsim 3$ SMGs are progenitors of $z \sim 2$ quiescent galaxies. The derived timescale does not depend strongly on the $z = 6$ upper limit adopted for the SMG redshift distribution. Adopting limits of $z = 5.5$ or $z = 7$ instead leads to timescales of 44 and 37 Myr, respectively. We note that the validity of the timescale calculation presented here relies on the assumption of a direct evolutionary connection between the two populations, implying that all $z = 2$ quiescent galaxies were once $z > 3$ SMGs and all $z > 3$ SMGs evolve into $z = 2$ quiescent galaxies.

3.6. Star Formation Rate and Timescale of $z = 2$ Quiescent Galaxies during Their Formation

We can infer a lower limit on the SFR of the $z = 2$ quiescent galaxies during their formation by assuming that they started forming stars at $z = 10$ and did so at a constant rate until their inferred formation redshifts. The minimum average SFR needed to acquire their observed stellar masses at $z = 2$ calculated in this way is $\langle SFR_{min} \rangle = 115 \pm 5 \, M_\odot \, \mathrm{yr}^{-1}$. This is a factor of > 3 larger than the observed average SFR in star-forming Lyman break galaxies (LBGs) at $z > 3$ (Carilli et al. 2008). Furthermore, the space density of $z \sim 2$ quiescent galaxies with $\log M_*/M_\odot > 11$ is 5, 10, and > 100 times larger than that of similar mass LBGs at $z = 4, 5$, and 6, respectively (Stark et al. 2009). Their progenitors must therefore have had much larger SFRs and are missing from LBG samples. This suggests that they must be dust-obscured starburst galaxies.
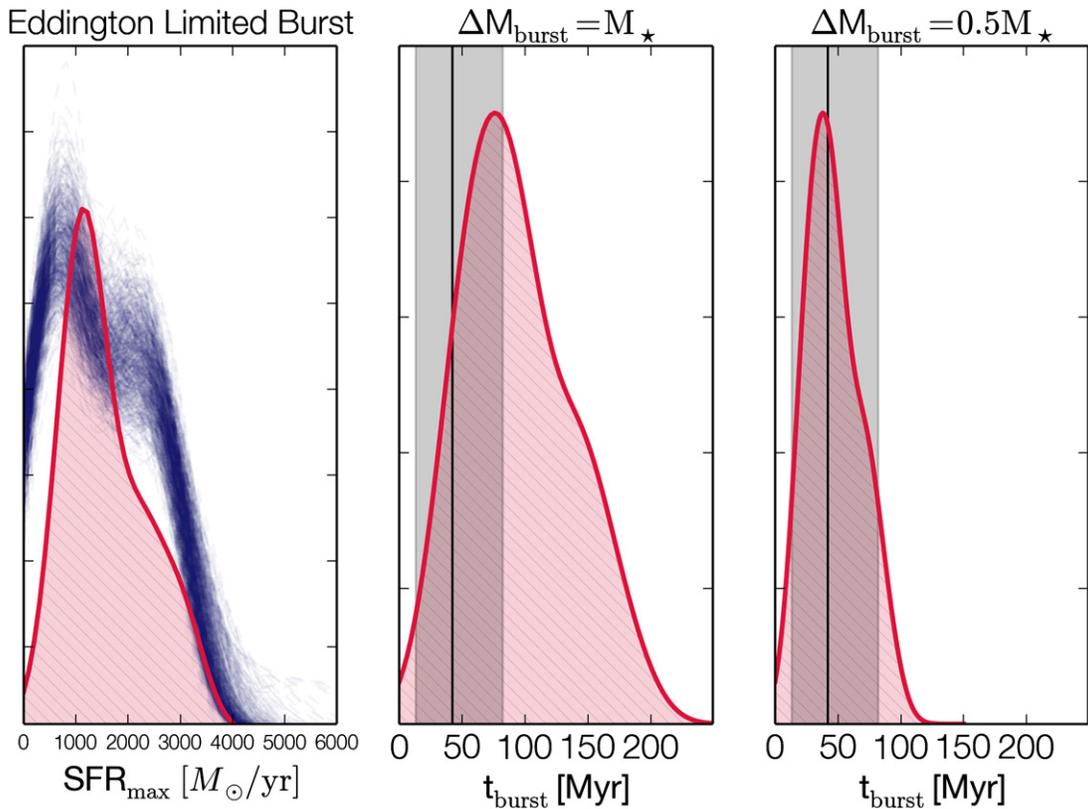
Figure 4. Comparison of the SFRs and starburst timescales derived for the $z > 3$ SMGs and $z \sim 2$ quiescent galaxies. Left: The red curve shows the probability density distribution (KDE) of SFRs of the $z \sim 2$ quiescent galaxies during their formation, calculated assuming they formed in Eddington-limited starbursts. The blue curves show probability distributions for 1000 realizations of ongoing SFRs in the $z > 3$ SMGs, estimated from their total infrared luminosity and associated errors. The two distributions span the same range, in support of an evolutionary connection between quiescent galaxies and SMGs. Middle: Probability density distribution of the duration of the cQG starbursts, calculated assuming that all their observed stellar mass formed in Eddington-limited bursts. The gray area indicates the constraints on the duty cycle of the SMG starbursts derived from their number density. Right: Same as the middle plot, but assuming that only half of the $z \sim 2$ quiescent galaxies' stellar mass formed in the Eddington-limited burst. The two independent measures $t_{\rm burst}$ are consistent, in agreement with $z > 3$ SMGs being progenitors of $z \sim 2$ quiescent galaxies.

(A color version of this figure is available in the online journal.)

Based on the observed line widths and compact spatial extent of molecular line-emitting regions, SMGs are often argued to be maximum starbursts, i.e, they form stars at a rate close to the Eddington limit. Assuming a spherical symmetric geometry, an isothermal sphere density structure, a small volume filling factor for molecular gas, and a Chabrier IMF based on Thompson et al. (2005), Younger et al. (2010) approximate this "maximum SFR" as

$$\text{SFR}_{\rm MAX} = 480\, \sigma_{400}^2\, D_{\rm kpc}\, \kappa_{100}^{-1} \quad [M_\odot\, \text{yr}^{-1}], \qquad (3)$$

where σ_{400} is the line-of-sight gas velocity dispersion in units of 400 km s^{-1}, κ_{100} is the opacity in units of cm^2 g^{-1} (usually taken to be ≈ 1; Murray et al. 2005; Thompson et al. 2005), and $D_{\rm kpc}$ is the characteristic physical scale of the starburst (usually approximated as the Gaussian FWHM of the line-emitting region). In Figure 4, the blue curves show probability distributions for 1000 realizations of ongoing SFRs in the $z > 3$ SMGs, estimated from their total infrared luminosity and associated errors, through Equation (1). The SMGs are forming stars at high rates 500–3000 $M_\odot$ yr^{-1}, close to the Eddington limit. For example, Younger et al. (2010) estimated the maximum SFR of AzTEC4 and AzTEC8 to be in the range of 1900–3800 $M_\odot$ yr^{-1}, comparable to the values derived here (see Table 2).

In the following, we investigate whether the observed properties of $z \sim 2$ quiescent galaxies are consistent with having

formed under such conditions. Assuming that $z \sim 2$ quiescent galaxies formed in Eddington-limited maximum starbursts, we can estimate the maximum SFR and the duration of this burst from the observed size, velocity dispersion, and stellar mass of the quiescent remnants. In Figure 4 the red curve shows the distribution of SFR$_{\rm MAX}$ for the sample of $z \sim 2$ quiescent galaxies described in Section 2.4, calculated from Equation (3), assuming $\kappa_{100} = 1$, $D_{\rm kpc} = 2\, r_{e,c}$ (where $r_{e,c}$ are the effective radii measured for the individual galaxies), and $\sigma_{400} = \langle \sigma \rangle / 400$ km s^{-1}, where $\langle \sigma \rangle = 363 \pm 100$ km s^{-1} is the mean velocity dispersion measured for $z \sim 2$ quiescent galaxies in the literature (Toft et al. 2012). We use this mean value as measured velocity dispersions for the K13 sample are not available.

There is a good general correspondence between the SFR$_{\rm MAX}$ distribution of quiescent $z \sim 2$ galaxies and the SFR distribution of $z \gtrsim 3$ SMGs. The SFR$_{\rm MAX}$ distribution peaks at higher SFRs than the observed distribution in $z \gtrsim 3$ SMGs, indicating that some of the $z \sim 2$ quiescent galaxies may have formed in starbursts with sub-Eddington SFRs. Also plotted in Figure 4(b) is the duration of this "maximum starburst"

$$t_{\rm burst} = \Delta M_\star / \text{SFR}_{\rm MAX} \qquad (4)$$

assuming a constant star formation rate SFR = SFR$_{\rm max}$ during the burst, and that all the stellar mass of the $z \sim 2$ quiescent galaxies was created during this burst, i.e., $\Delta M_\star = M_\star$. While
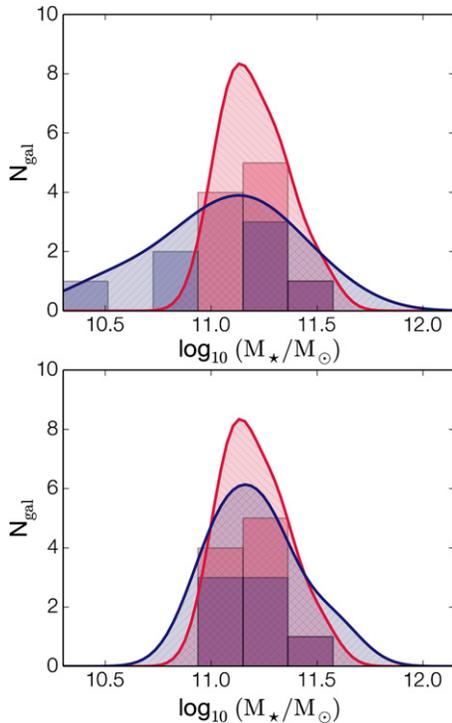
Figure 5. Red histograms show the distribution of stellar masses in $\log(M/M_\odot) > 11$ quiescent galaxies at $z \sim 2$. In the top panel the blue histogram shows the distribution of stellar masses in the $z \gtrsim 3$ SMGs. In the bottom panel the blue histogram shows the final stellar masses of the $z \gtrsim 3$ SMGs assuming that $10\% \pm 5\%$ of their derived gas mass is turned into stars during the remainder of the ongoing starburst (Hayward et al. 2011).

(A color version of this figure is available in the online journal.)

consistent within the errors, the mean derived timescale for Eddington-limited starbursts is about a factor of two longer than the starburst timescale derived from comparing comoving number densities. This can be accounted for by changing some of the assumptions, e.g., if the SMG starbursts are triggered by major mergers, a fraction of the stellar mass must have been formed in the progenitor galaxies prior to the merger. In Figure 4(c) we show that if we assume that only half of the observed stellar mass in $z \sim 2$ quiescent galaxies was created in a $z \gtrsim 3$ Eddington-limited starburst, i.e., $\Delta M_\star = 0.5\, M_\star$, there is excellent agreement between the derived timescales, consistent with the idea that $z \gtrsim 3$ SMGs are the progenitors of $z \sim 2$ quiescent galaxies. Interestingly, this is consistent with the results of Michałowski et al. (2010b), who found that on average $\sim 45\%$ of the stellar mass in a sample of $z > 4$ SMGs was formed in their ongoing starbursts. If half the stellar mass formed prior to the merger that ignites the SMG starburst, an implication is that the merger progenitors must have been gas-rich star-forming galaxies, in agreement with the high gas fractions found in high redshift star-forming galaxies (Tacconi et al. 2013).

3.7. Additional Stellar Mass Growth and Quenching of the $z \gtrsim 3$ SMGs

The similar mass–size distribution of the $z \gtrsim 3$ SMGs and $z \sim 2$ quiescent galaxies is in agreement with what one would expect if the $z \gtrsim 3$ SMGs evolve passively into $z \sim 2$ quiescent galaxies, after they have been quenched. Prior to the quenching, however, the ongoing starburst will increase the stellar masses of the galaxies. In Figure 5 we show that the distribution of stellar masses in the $z \gtrsim 3$ SMGs is broader than that of

$\log(M/M_\odot) > 11$ quiescent galaxies at $z \sim 2$. We can estimate the growth of stellar mass in the individual $z \gtrsim 3$ SMGs from their gas masses, inferred from the FIR SED fits (see Table 2). From these we can estimate the final stellar masses of the $z \gtrsim 3$ SMGs if we assume a star formation efficiency, i.e, the fraction of gas that is turned into stars during the starburst. In the simulations of Hayward et al. (2011) the gas fraction decreases from 45% to 40% in isolated disks and from 17.5% to 15% in merging galaxies, from the peak of the starburst to when it ends, which corresponds to a decrease in gas mass of 5% and 15% during this time. If we assume that this gas is turned into stars, and that we are observing the SMGs at the peak of their starburst, the models thus indicate that $\sim 10\% \pm 5\%$ of the observed gas mass in the $z \gtrsim 3$ SMGs will be turned into stars during the remainder of the burst. In Figure 5 we compare the final stellar mass distribution of the $z \gtrsim 3$ SMGs with that of quiescent $z \sim 2$ quiescent galaxies, assuming that 10% of the derived gas mass in the $z \gtrsim 3$ SMGs is turned into stars before the starbursts are quenched. The two distributions are similar, with a K-S test statistic of 0.33 and a probability of 67%, in agreement with a direct evolutionary link between the two populations. The mass increase from the time the SMGs are observed up to the end of the starburst will likely not significantly increase the effective radii as the process is highly dissipative, resulting in a slight horizontal shift in the $M_\star - r_e$ plane (blue points in Figure 3). The continued starbursts and subsequent quenching may also provide the mechanism needed to transform the observed low-n disk-like surface brightness profiles observed in SMGs to the higher n bulge-like profiles observed in quiescent galaxies at $z \sim 2$ (Wuyts et al. 2011; Szomoru et al. 2011; Bell et al. 2012). Most of the stellar mass will be added in the nuclear regions of the SMGs, which is likely highly obscured by dust. Once the quenching sets in and most of the dust is destroyed or blown away, a more centrally concentrated surface brightness distribution could be revealed. Note that if, as assumed here, only 10% of the large derived gas mass in the $z \gtrsim 3$ SMGs is turned into stars during the remainder of the burst, the following quenching mechanism must be highly efficient at heating or expelling the substantial amounts of leftover gas. A possible mechanism for expelling the gas is through outflows, driven by strong winds associated with the maximum starbursts. Tentative evidence for such outflows has recently been observed in the 163 μm OH line profile in an SMG at $z = 6.3$ (Riechers et al. 2013). We stress that the large systematic uncertainties on the derived stellar masses for the SMGs could potentially influence our conclusions.

4. SUMMARY AND DISCUSSION

4.1. The Link between $z \gtrsim 3$ SMGs and $z \sim 2$ Compact, Quiescent Galaxies

In this article we presented evidence for a direct evolutionary connection between two of the most extreme galaxy types in the universe, the highest redshift ($z \gtrsim 3$) SMGs that host some of the most intense starbursts known and quiescent galaxies at $z \sim 2$ that host the densest conglomerations of stellar mass known. The comparison was motivated by the recent discovery of a significant population of SMGs at $3 < z < 6$ and high-resolution imaging and spectroscopic studies of $z \sim 2$ quiescent galaxies that show that the majority of their stars likely formed in massive nuclear, possibly dust-enshrouded, starbursts in this redshift range. From a unique flux-limited statistical sample of $z \gtrsim 3$ SMGs in the COSMOS field, we have put robust
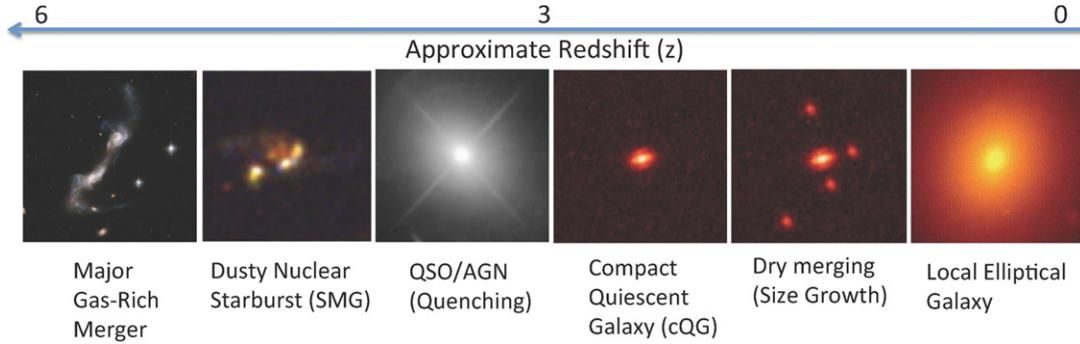
6   3   0

Approximate Redshift (z)

| Major Gas-Rich Merger | Dusty Nuclear Starburst (SMG) | QSO/AGN (Quenching) | Compact Quiescent Galaxy (cQG) | Dry merging (Size Growth) | Local Elliptical Galaxy |

Figure 6. Schematic illustration of the formation and evolutionary sequence for massive galaxies advocated in this article.
(A color version of this figure is available in the online journal.)

constraints on their comoving number density, which we then put in the context of the comoving number densities of quiescent galaxies of similar mass at $z \sim 2$. If $z \gtrsim 3$ SMGs are progenitors of $z \sim 2$ quiescent galaxies, then our data imply that the SMG duty cycle must be $t_{\mathrm{burst}} = 42^{+40}_{-29}$ Myr, where the error bars include our best estimates of the effects of cosmic variance, photometric redshift errors, and incompleteness. This timescale is independent from, but in good agreement with, estimates based on SMG gas depletion timescales $t_{\mathrm{burst}} \sim 40$–$200$ Myr, estimates from hydrodynamical merger simulations $t_{\mathrm{burst}} \sim 50$ Myr (e.g., Mihos & Hernquist 1996; Cox et al. 2008), and estimates based on the time compact starburst galaxies spend above the main sequence of star formation $t_{\mathrm{burst}} < 70$ Myr (Wuyts et al. 2011). Importantly, as our estimate of the SMG starburst timescale is based only on number density arguments, it is relatively independent of assumptions of the underlying stellar IMF, which is a large potential systematic uncertainty, e.g., in depletion timescale estimates.

Based on stellar masses derived from UV–MIR photometry and sizes derived from deep NIR imaging, we have shown that the mass–size distribution of the $z \gtrsim 3$ galaxies is remarkably similar to that observed for compact quiescent massive galaxies at $z \sim 2$, and that it has similar mean internal stellar mass surface densities $\langle \log(\Sigma) \rangle \sim 9.8\ M_\odot\ \mathrm{kpc}^{-2}$. The surface brightness distributions of the $z \gtrsim 3$ SMGs are best fit by Sersic models with low Sersic n parameters, which is typical of local star-forming disk galaxies or mergers. The majority also show multiple components or irregularities indicative of ongoing merging and/or clumpy structures.

Many similarities between $z \sim 2$ quiescent galaxies and SMGs exist: they have similar stellar masses, characteristic internal velocities, dynamical masses, sizes, correlation lengths, etc. Millimeter measurements of $z \gtrsim 3$ SMGs in continuum and CO show signatures of merging or rotation (Younger et al. 2008, 2010; Riechers et al. 2011b, 2011c), with molecular emission line widths in the range of 300–700 km s^{-1} (with a few outliers) and a mean $\langle \mathrm{FWHM} \rangle = 456 \pm 253$ km s^{-1} (Schinnerer et al. 2008; Daddi et al. 2009a; Coppin et al. 2010; Riechers et al. 2010, 2011b, 2011c; Swinbank et al. 2012; Walter et al. 2012) similar to stellar velocity dispersions $\sigma = 300$–500 km s^{-1} measured in $z \sim 2$ quiescent galaxies. For example, for AzTEC 3, at $z = 5.3$, Riechers et al. (2010) measured a CO line width of 487 km s^{-1} and a gas depletion timescale of 30 Myr, similar to the SMG starburst timescale derived here. At the depth and resolution of the present data, it is impossible to make strong claims about how many $z \gtrsim 3$ SMGs are in the process of

merging. However, all the detected galaxies show evidence of close companions, multiple components, or clumpy structure and have low derived Sersic indices, which is consistent with expectations for merging galaxies. In particular, the two galaxies with *HST*/WFC3 data appear to be major mergers.

The evidence presented in this article is in support of a direct evolutionary connection between $z \gtrsim 3$ SMGs, through compact quiescent galaxies at $z \sim 2$ to giant elliptical galaxies in the local universe. In this scenario (illustrated in Figure 6) gas-rich, major mergers in the early universe trigger nuclear dust-enshrouded starbursts,[24] which on average last 42^{+40}_{-29} Myr, followed by star formation quenching, either due to gas exhaustion, feedback from the starburst, or the ignition of an AGN, leaving behind compact stellar remnants to evolve passively for about a Gyr into the compact quiescent galaxies we observe at $z \sim 2$. Over the next 10 Gyr, these then grow gradually, primarily through minor merging, into local elliptical galaxies.

4.2. Connection to Compact Star-forming Galaxies at 2.5 < z < 3

Barro et al. (2013) found a population of relatively massive ($\log(M/M_\odot > 10$) compact star-forming galaxies (cSFGs) at $1.4 < z < 3$, which show evidence of quenching beginning to set in (i.e., lower specific SFRs than typical star-forming galaxies and increased AGN fractions). Their masses, sizes, and number densities (which increase with decreasing redshift at the same time the number density of quiescent galaxies increases) suggest that the highest redshift examples of these may be progenitors of compact quiescent $z \sim 2$ galaxies. These galaxies are thus good candidates for transition objects in the evolutionary sequence suggested here between the $z \gtrsim 3$ SMGs and the $z \sim 2$ quiescent galaxies. The comoving number density of the most massive cSFGs ($\log(M/M_\odot > 10.8$) at $2.5 < z < 3$ is $\sim (5.4 \pm 2.5) \times 10^{-5}$ Mpc^{-3}, which is comparable to the number density for $z \sim 2$ quiescent galaxies. However, the cSFGs are not massive enough to be descendants of the brightest $z \gtrsim 3$ SMGs or progenitors of most of the massive $z \sim 2$ quiescent galaxies considered here, as none of the cSFGs have $\log(M/M_\odot) > 11$ (M. Barro 2013, private communication) but are likely decedents of less intense starbursts at $z \gtrsim 3$ and progenitors of slightly lower mass quiescent $z = 2$ galaxies.

_____

[24] The SMG image in the figure is adopted from Targett et al. (2013).

4.3. Caveats and Outlook

One of the largest uncertainties in the derivables for the $z \gtrsim 3$ SMG sample is associated with their stellar masses. As extensively discussed in Michałowski et al. (2012a), stellar masses for SMGs are highly dependent on the assumed star formation history and may differ by up to ± 0.5 dex given different assumptions and models. Dynamical mass considerations may set an upper limit to stellar masses. However, the $z \gtrsim 3$ SMG samples with available dynamical mass estimates are still sparse, as well as subject to their own biases.

The sample of $z \gtrsim 3$ SMGs is still small and only partially spectroscopically confirmed. Future, larger and deeper mm surveys, over multiple fields, will allow for better constraints on the evolution of the comoving number density of starburst galaxies, to the highest redshifts, and to study the effects of cosmic variance. This will allow for more detailed tests and modeling of the proposed scenario in different redshifts and mass bins, rather than in the single mass bin and two redshift ranges that we are limited to with the present data. For example, the proposed scenario implies that the significant population of $z \sim 2$ SMGs should evolve into compact, ~ 1 Gyr old, massive poststarburst galaxies at $z \sim 1.5$. Interestingly, Bezanson et al. (2012) recently published a spectroscopic sample of galaxies with exactly these properties. Similarly, if compact quiescent galaxies at $z \gtrsim 3$ are found in the future, the properties of these should match those of the highest redshift $z > 5$ SMGs. With deeper data it will also be possible to push to lower SFRs and not only consider the most extreme starbursts. This will likely provide a way of fitting the $2.5 < z < 3$ cSFGs discussed in Section 4.2 into the evolutionary picture.

Cosmological surface brightness dimming and the large amounts (and unknown distribution) of dust in SMGs make them extremely faint in the rest-frame UV and optical and likely bias the sizes measured, even in very deep NIR imaging data. However, we do note that one of the galaxies in our sample (AzTEC1) has been resolved in high-resolution submillimeter imaging (Younger et al. 2008), with a derived extent of $0\rlap{.}''1$–$0\rlap{.}''2$ and corresponding to a physical size of 1.3–2.7 kpc, which is consistent with the constraints on the effective radius we measure from the UltraVISTA data ($r_e < 2.6$ kpc; see Table 1). ALMA will greatly improve estimates of the sizes of high-redshift SMGs through high-resolution observations of the rest-frame FIR dust continuum. We have argued in this article that the observed structural properties are consistent with the SMGs being disks or mergers, but the constraints are uncertain due to the relatively low S/N and spatial resolution of the images, e.g., the Sersic n parameters and effective radii could be underestimated due to obscuration by dust and cosmological surface brightness dimming. With ALMA it will be straightforward to determine redshifts from molecular lines and constrain the internal dynamics of the galaxies, e.g., estimate velocity dispersions and rotational velocities and search for evidence of merging. This will provide powerful diagnostics to help map the transformation of the most massive galaxies in the universe from enigmatic starbursts at cosmic dawn to dead remnants a few gigayears later.

REFERENCES

Aretxaga, I., Wilson, G. W., Aguilar, E., et al. 2011, MNRAS, 415, 3831
Austermann, J. E., Aretxaga, I., Hughes, D. H., et al. 2009, MNRAS, 393, 1573
Barro, G., Faber, S. M., Pérez-González, P. G., et al. 2013, ApJ, 765, 104
Bell, E. F., van der Wel, A., Papovich, C., et al. 2012, ApJ, 753, 167
Bertoldi, F., Carilli, C., Aravena, M., et al. 2007, ApJS, 172, 132
Bezanson, R., van Dokkum, P., & Franx, M. 2012, ApJ, 760, 62
Bezanson, R., van Dokkum, P. G., Tal, T., et al. 2009, ApJ, 697, 1290
Blain, A. W., Chapman, S. C., Smail, I., & Ivison, R. 2004, ApJ, 611, 725
Bolatto, A. D., Leroy, A. K., Jameson, K., et al. 2011, ApJ, 741, 12
Brammer, G. B., Whitaker, K. E., van Dokkum, P. G., et al. 2011, ApJ, 739, 24
Bruzual, G., & Charlot, S. 2003, MNRAS, 344, 1000
Capak, P., Carilli, C. L., Lee, N., et al. 2008, ApJL, 681, L53
Capak, P. L. 2009, BAAS, 41, 708
Capak, P. L., Scoville, N. Z., Sanders, D. B., et al. 2010, BAAS, 42, 235
Carilli, C. L., Daddi, E., Riechers, D., et al. 2010, ApJ, 714, 1407
Carilli, C. L., Hodge, J., Walter, F., et al. 2011, ApJL, 739, L33
Carilli, C. L., Lee, N., Capak, P., et al. 2008, ApJ, 689, 883
Carollo, C. M., Bschorr, T. J., Renzini, A., et al. 2013, ApJ, 773, 112
Cassata, P., Giavalisco, M., Williams, C. C., et al. 2013, ApJ, 775, 106
Chabrier, G. 2003, ApJL, 586, L133
Chapman, S. C., Blain, A. W., Smail, I., & Ivison, R. J. 2005, ApJ, 622, 772
Cimatti, A., Cassata, P., Pozzetti, L., et al. 2008, A&A, 482, 21
Cimatti, A., Nipoti, C., & Cassata, P. 2012, MNRAS, 422, L62
Combes, F., Rex, M., Rawle, T. D., et al. 2012, A&A, 538, L4
Coppin, K. E. K., Chapman, S. C., Smail, I., et al. 2010, MNRAS, 407, L103
Coppin, K. E. K., Swinbank, A. M., Neri, R., et al. 2008, MNRAS, 389, 45
Cox, P., Krips, M., Neri, R., et al. 2011, ApJ, 740, 63
Cox, T. J., Jonsson, P., Somerville, R. S., Primack, J. R., & Dekel, A. 2008, MNRAS, 384, 386
da Cunha, E., Charlot, S., & Elbaz, D. 2008, MNRAS, 388, 1595
Daddi, E., Dannerbauer, H., Krips, M., et al. 2009a, ApJL, 695, L176
Daddi, E., Dannerbauer, H., Stern, D., et al. 2009b, ApJ, 694, 1517
Daddi, E., Renzini, A., Pirzkal, N., et al. 2005, ApJ, 626, 680
Damjanov, I., Abraham, R. G., Glazebrook, K., et al. 2011, ApJL, 739, L44
Dekel, A., Birnboim, Y., Engel, G., et al. 2009, Natur, 457, 451
Draine, B. T., & Li, A. 2007, ApJ, 657, 810
Dwek, E., Staguhn, J. G., Arendt, R. G., et al. 2011, ApJ, 738, 36
Erb, D. K., Shapley, A. E., Pettini, M., et al. 2006, ApJ, 644, 813
Franx, M., van Dokkum, P. G., Schreiber, N. M. F., et al. 2008, ApJ, 688, 770
Frayer, D. T., Ivison, R. J., Scoville, N. Z., et al. 1999, ApJL, 514, L13
Fu, H., Cooray, A., Feruglio, C., et al. 2013, Natur, 498, 338
Genzel, R., Tacconi, L. J., Combes, F., et al. 2012, ApJ, 746, 69
Greve, T. R., Bertoldi, F., Smail, I., et al. 2005, MNRAS, 359, 1165
Grogin, N. A., Kocevski, D. D., Faber, S. M., et al. 2011, ApJS, 197, 35
Hayward, C. C., Kereš, D., Jonsson, P., et al. 2011, ApJ, 743, 159
Hickox, R. C., Wardlow, J. L., Smail, I., et al. 2012, MNRAS, 421, 284
Hodge, J. A., Carilli, C. L., Walter, F., Daddi, E., & Riechers, D. 2013a, ApJ, 776, 22
Hodge, J. A., Carilli, C. L., Walter, F., et al. 2012, ApJ, 760, 11
Hodge, J. A., Karim, A., Smail, I., et al. 2013b, ApJ, 768, 91
Hopkins, P. F., Somerville, R. S., Hernquist, L., et al. 2006, ApJ, 652, 864
Iglesias-Páramo, J., Buat, V., Hernández-Fernández, J., et al. 2007, ApJ, 670, 279
Ivison, R. J., Papadopoulos, P. P., Smail, I., et al. 2011, MNRAS, 412, 1913
Ivison, R. J., Swinbank, A. M., Smail, I., et al. 2013, ApJ, 772, 137
Kennicutt, R. C., Jr. 1998, ARA&A, 36, 189
Kneib, J.-P., Neri, R., Smail, I., et al. 2005, A&A, 434, 819

Knudsen, K. K., Kneib, J.-P., Richard, J., Petitpas, G., & Egami, E. 2010, ApJ, 709, 210

Koekemoer, A. M., Faber, S. M., Ferguson, H. C., et al. 2011, ApJS, 197, 36

Kriek, M., van Dokkum, P. G., Labbé, I., et al. 2009, ApJ, 700, 221

Krogager, J.-K., Zirm, A. W., Toft, S., Man, A., & Brammer, G. 2013, arXiv:1309.6316

Le Floc'h, E., Aussel, H., Ilbert, O., et al. 2009, ApJ, 703, 222

Leroy, A. K., Bolatto, A., Gordon, K., et al. 2011, ApJ, 737, 12

Lotz, J. M., Jonsson, P., Cox, T. J., & Primack, J. R. 2010, MNRAS, 404, 575

Lutz, D., Poglitsch, A., Altieri, B., et al. 2011, A&A, 532, A90

Magdis, G. E., Daddi, E., Elbaz, D., et al. 2011, ApJL, 740, L15

Magdis, G. E., Daddi, E., Sargent, M., et al. 2012, ApJL, 758, L9

Magnelli, B., Elbaz, D., Chary, R. R., et al. 2009, A&A, 496, 57

Magnelli, B., Saintonge, A., Lutz, D., et al. 2012, A&A, 548, A22

McCracken, H. J., Milvang-Jensen, B., Dunlop, J., et al. 2012, A&A, 544, A156

Michałowski, M., Hjorth, J., & Watson, D. 2010a, A&A, 514, A67

Michałowski, M. J., Dunlop, J. S., Cirasuolo, M., et al. 2012a, A&A, 541, A85

Michałowski, M. J., Dunlop, J. S., Ivison, R. J., et al. 2012b, MNRAS, 426, 1845

Michałowski, M. J., Watson, D., & Hjorth, J. 2010b, ApJ, 712, 942

Mihos, J. C., & Hernquist, L. 1996, ApJ, 464, 641

Moster, B. P., Somerville, R. S., Newman, J. A., & Rix, H.-W. 2011, ApJ, 731, 113

Murray, N., Quataert, E., & Thompson, T. A. 2005, ApJ, 618, 569

Naab, T., Johansson, P. H., & Ostriker, J. P. 2009, ApJL, 699, L178

Naab, T., Johansson, P. H., Ostriker, J. P., & Efstathiou, G. 2007, ApJ, 658, 710

Neri, R., Genzel, R., Ivison, R. J., et al. 2003, ApJL, 597, L113

Newman, A. B., Ellis, R. S., Bundy, K., & Treu, T. 2012, ApJ, 746, 162

Oliver, S. J., Bock, J., Altieri, B., et al. 2012, MNRAS, 424, 1614

Olsen, K. P., Rasmussen, J., Toft, S., & Zirm, A. W. 2013, ApJ, 764, 4

Onodera, M., Daddi, E., Gobat, R., et al. 2010, ApJL, 715, L6

Onodera, M., Renzini, A., Carollo, M., et al. 2012, ApJ, 755, 26

Oser, L., Naab, T., Ostriker, J. P., & Johansson, P. H. 2012, ApJ, 744, 63

Peng, C. Y., Ho, L. C., Impey, C. D., & Rix, H.-W. 2002, AJ, 124, 266

Ricciardelli, E., Trujillo, I., Buitrago, F., & Conselice, C. J. 2010, MNRAS, 406, 230

Riechers, D. A. 2013, ApJL, 765, L31

Riechers, D. A., Bradford, C. M., Clements, D. L., et al. 2013, Natur, 496, 329

Riechers, D. A., Capak, P. L., Carilli, C. L., et al. 2010, ApJL, 720, L131

Riechers, D. A., Carilli, L. C., Walter, F., et al. 2011a, ApJL, 733, L11

Riechers, D. A., Cooray, A., Omont, A., et al. 2011b, ApJL, 733, L12

Riechers, D. A., Hodge, J., Walter, F., Carilli, C. L., & Bertoldi, F. 2011c, ApJL, 739, L31

Riechers, D. A., Walter, F., Carilli, C. L., Bertoldi, F., & Momjian, E. 2008, ApJL, 686, L9

Rieke, G. H., Young, E. T., Engelbracht, C. W., et al. 2004, ApJS, 154, 25

Roseboom, I. G., Oliver, S. J., Kunz, M., et al. 2010, MNRAS, 409, 48

Sanders, D. B., Salvato, M., Aussel, H., et al. 2007, ApJS, 172, 86

Sanders, D. B., Soifer, B. T., Elias, J. H., et al. 1988, ApJ, 325, 74

Schaerer, D., de Barros, S., & Sklias, P. 2013, A&A, 549, A4

Schinnerer, E., Capak, P., Carilli, C. L., Scoville, N. Z., & COSMOS Collaboration 2009, BAAS, 41, 708

Schinnerer, E., Carilli, C. L., Capak, P., et al. 2008, ApJL, 689, L5

Scott, K. S., Austermann, J. E., Perera, T. A., et al. 2008, yCat, 738, 52225

Sheth, K., Blain, A. W., Kneib, J.-P., et al. 2004, ApJL, 614, L5

Silva, L., Granato, G. L., Bressan, A., & Danese, L. 1998, ApJ, 509, 103

Smolčić, V., Aravena, M., Navarrete, F., et al. 2012a, A&A, 548, A4

Smolčić, V., Capak, P., Ilbert, O., et al. 2011, ApJL, 731, L27

Smolčić, V., Navarrete, F., Aravena, M., et al. 2012b, ApJS, 200, 10

Stark, D. P., Ellis, R. S., Bunker, A., et al. 2009, ApJ, 697, 1493

Swinbank, M., Smail, I., Karim, A., et al. 2012, Msngr, 149, 40

Szomoru, D., Franx, M., Bouwens, R. J., et al. 2011, ApJL, 735, L22

Szomoru, D., Franx, M., & van Dokkum, P. G. 2012, ApJ, 749, 121

Tacconi, L. J., Genzel, R., Smail, I., et al. 2008, ApJ, 680, 246

Tacconi, L. J., Neri, R., Chapman, S. C., et al. 2006, ApJ, 640, 228

Tacconi, L. J., Neri, R., Genzel, R., et al. 2013, ApJ, 768, 74

Targett, T. A., Dunlop, J. S., Cirasuolo, M., et al. 2013, MNRAS, 432, 2012

Thomas, D., Maraston, C., Bender, R., & Mendes de Oliveira, C. 2005, ApJ, 621, 673

Thompson, T. A., Quataert, E., & Murray, N. 2005, ApJ, 630, 167

Toft, S., Franx, M., van Dokkum, P., et al. 2009, ApJ, 705, 255

Toft, S., Gallazzi, A., Zirm, A., et al. 2012, ApJ, 754, 3

Toft, S., van Dokkum, P., Franx, M., et al. 2005, ApJL, 624, L9

Toft, S., van Dokkum, P., Franx, M., et al. 2007, ApJ, 671, 285

Treister, E., Schawinski, K., Urry, C. M., & Simmons, B. D. 2012, ApJL, 758, L39

Trujillo, I., Förster Schreiber, N. M., Rudnick, G., et al. 2006, ApJ, 650, 18

van de Sande, J., Kriek, M., Franx, M., et al. 2011, ApJL, 736, L9

van de Sande, J., Kriek, M., Franx, M., et al. 2012, ArXiv e-prints

van Dokkum, P. G., Franx, M., Kriek, M., et al. 2008, ApJL, 677, L5

van Dokkum, P. G., Whitaker, K. E., Brammer, G., et al. 2010, ApJ, 709, 1018

Wake, D. A., Whitaker, K. E., Labbé, I., et al. 2011, ApJ, 728, 46

Walter, F., Decarli, R., Carilli, C., et al. 2012, Natur, 486, 233

Wardlow, J. L., Smail, I., Coppin, K. E. K., et al. 2011, MNRAS, 415, 1479

Williams, R. J., Quadri, R. F., Franx, M., et al. 2010, ApJ, 713, 738

Wuyts, S., Cox, T. J., Hayward, C. C., et al. 2010, ApJ, 722, 1666

Wuyts, S., Förster Schreiber, N. M., van der Wel, A., et al. 2011, ApJ, 742, 96

Younger, J. D., Fazio, G. G., Ashby, M. L. N., et al. 2010, MNRAS, 407, 1268

Younger, J. D., Fazio, G. G., Huang, J.-S., et al. 2007, ApJ, 671, 1531

Younger, J. D., Fazio, G. G., Huang, J.-S., et al. 2009, ApJ, 704, 803

Younger, J. D., Fazio, G. G., Wilner, D. J., et al. 2008, ApJ, 688, 59

Yun, M. S., Scott, K. S., Guo, Y., et al. 2012, MNRAS, 420, 957